

A batch fabricated biomimetic dry adhesive

Michael T Northen^{1,3} and Kimberly L Turner²

¹ Materials Department, University of California at Santa Barbara, Santa Barbara, CA 93106, USA

² Mechanical and Environmental Engineering Department, University of California at Santa Barbara, Santa Barbara, CA 93106, USA

E-mail: north@engineering.ucsb.edu

Received 3 February 2005, in final form 1 April 2005

Published 17 May 2005

Online at stacks.iop.org/Nano/16/1159

Abstract

The fine hair adhesive system found in nature is capable of reversibly adhering to just about any surface. This dry adhesive, best demonstrated in the pad of the gecko, makes use of a multilevel conformal structure to greatly increase inelastic surface contact, enhancing short range interactions and producing significant amounts of attractive forces. Recent work has attempted to reproduce and test the terminal submicrometre ‘hairs’ of the system. Here we report the first batch fabricated multi-scale conformal system to mimic nature’s dry adhesive. The approach makes use of massively parallel MEMS processing technology to produce 20–150 μm platforms, supported by single slender pillars, and coated with $\sim 2 \mu\text{m}$ long, $\sim 200 \text{ nm}$ diameter, organic looking polymer nanorods, or ‘organorods’. To characterize the structures a new mesoscale nanoindenter adhesion test technique has been developed. Experiments indicate significantly improved adhesion with the multiscale system. Additional processing caused a hydrophilic to hydrophobic transformation of the surface and testing indicated further improvement in adhesion.

(Some figures in this article are in colour only in the electronic version)

1. Introduction

Used by insects and lizards (including flies, crickets, beetles, spiders, geckos and anoles) to climb wet or dry, vertical and even inverted surfaces, the fine hair adhesive system is an excellent example of convergent evolution in biology [1–8]. Recently, much work has been done to obtain better understanding of the science of the sticking of this fine hair adhesive motif [6–12]. Experimental evidence has shown that the adhesion is primarily due to short range weak van der Waals interactions between the fine hairs on the adhering surface and the target surface [7]. In order for these ‘weak’ forces to become significant the adhesive surface must create a large amount of intimate surface contact to the binding surface. In the case of the *Gekko gekko*, that can weigh up to 300 g, this is achieved by a multilevel conformal system consisting of toes containing blood sinuses supporting rows

of imbricated lamellae with densely packed keratinous setae approximately 100 μm in length, which split into finer 200 nm in diameter bristles [2]. Each element of the system, from the toe to the terminal bristles, provides another scale of surface conformation, from the centimetre mesoscale (toe) down to the nanoscale (bristles). This inelastic surface conformation allows the gecko’s foot to create a large amount of surface contact, without introducing repulsive restoring force from the surface, producing a significant amount of surface adhesion through short range interactions [11].

Prior work has focused on mimicking the terminal bristle component of the adhesive by fabricating arrays of polymeric nanorods on solid substrate [7, 13, 14]. While individual nanorods demonstrated expected amounts of adhesion, larger arrays failed to produce larger amounts of adhesion—unless removed from the substrate and placed on a compliant backing [14], showing the need for multiscale compliance. Additionally, the arrays of nanorods showed reduced adhesion

³ Author to whom any correspondence should be addressed.

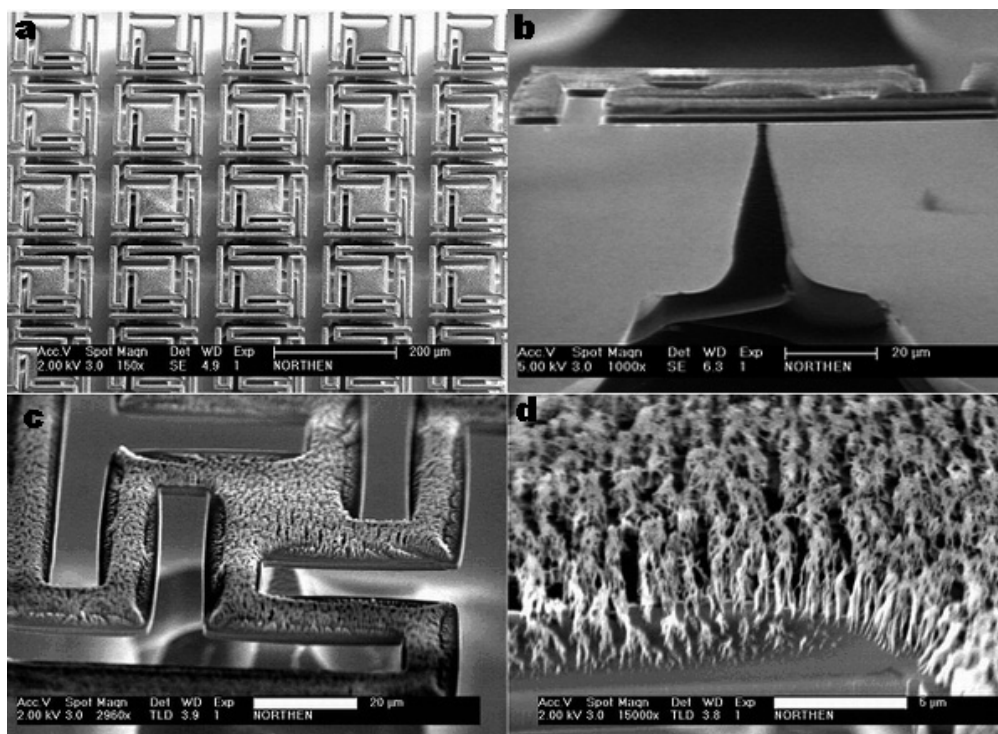


Figure 1. Electron micrographs of silicon dioxide platforms supported by single slender pillars and coated with polymeric organorods. The structures are batch fabricated using standard bulk microfabrication techniques requiring only a single lithography step. (a) Array of four-fingered platform structures. Scale bar: 200 μm . (b) Profile view of an organorod coated silicon dioxide platform supported by a single-crystal silicon pillar. Scale bar: 20 μm . (c) Magnified view of the multiscale system. Scale bar: 20 μm . The integration of the ~ 200 nm diameter organorods with the 150 μm platform structures provides enhanced surface conformation. (d) High resolution electron micrograph of the edge of an organorod coated finger. Scale bar: 5 μm .

with use, due to bunching and contamination [14], suggesting the reason for the superhydrophobic nature of the gecko pad.

In the last two decades the emerging field of microelectromechanical systems (MEMS) has created a variety of microdevices. These devices offer distinct advantages due to their small size, particularly in sensing. Microsensors have been developed for location determination, chemical sensing, mass sensing, pressure sensing and inertial sensing [15–22]. One key issue is how to deploy these microdevices. The ability to incorporate an adhesive into the fabrication process and have that adhesive stick to virtually any surface, in any environment, offers a significant technological advancement. Another key aspect in both microdevices and nanodevices is the integration into complete device architectures. As device architectures are miniaturized and span multiple disciplines (biology, integrated circuits, MEMS etc) new strategies for assembly and integration will be needed. The ability to pattern an adhesive with potentially submicrometre precision for chip recognition or self-assembly strategies will be a valuable tool.

2. Fabrication

In this work, a chip-scale batch fabricated multiscale conformal system has been produced. The microelectromechanical systems (MEMS)-based approach allows for batch fabrication and chip integration of the adhesive. The multiscale structures consist of arrays of organic looking photoresist nanorods,

‘organorods’, approximately 2 μm tall and 50–200 nm in diameter, atop photolithographically defined 2 μm thick silicon dioxide platforms 100–150 μm on a side (figure 1). The platforms of varying geometries are supported by single high aspect ratio pillars down to 1 μm in diameter and with heights up to ~ 50 μm (figure 2). The structures are fabricated out of four-inch single-crystal silicon wafers in the (100) orientation using standard bulk micromachining techniques [23]. Using a wet oxidation process at 1100 $^{\circ}\text{C}$, 2 μm of silicon dioxide is grown on the silicon wafer. To define the top platform geometry standard stepper photolithography in an i-line stepper is performed using a positive resist, Shipley SPR 220-7. The resist is then used as an etch mask in an ICP etcher with CHF_3 chemistry to vertically etch through the silicon dioxide to the silicon. The exposed silicon is then etched using the BoschTM process, also known as deep reactive ion etching (DRIE), where the plasma is cycled between a highly reactive SF_6 gas and a hydrocarbon forming CF_4 species, creating high aspect ratio vertical cavities. The depth of these cavities can be controlled depending on the desired final aspect ratio of the pillars. Directly following the deep etch, an extended SF_6 etch is used to isotropically etch the silicon. Since the reactive etch is significantly more selective to the silicon than the silicon dioxide (or photoresist) the platforms are undercut from all directions leaving behind only a single pillar in the middle (figure 2). By controlling the duration of the release it is possible to control the final size of the pillars supporting the platforms [23].

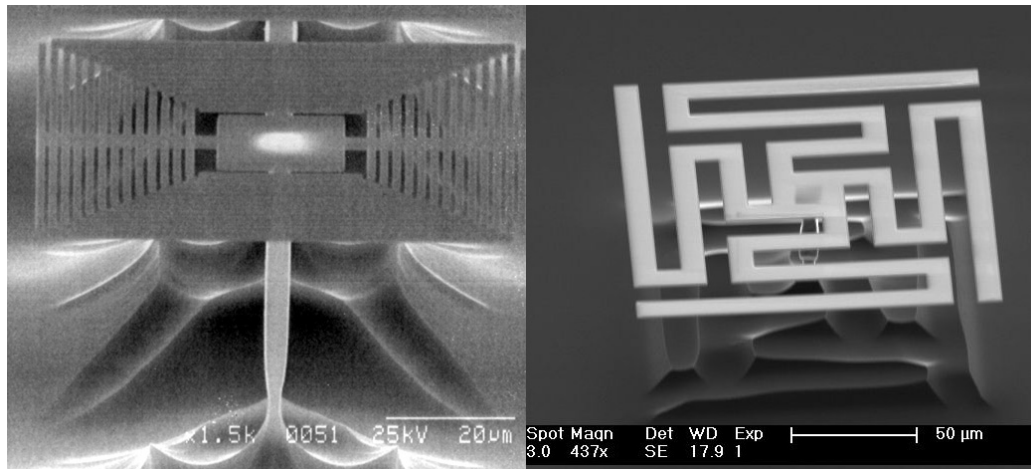


Figure 2. Silicon dioxide platforms supported by single high aspect ratio pillars etched out of single-crystal silicon using a modified microfabrication technique. Scale bars: 20 and 50 μm left and right respectively.

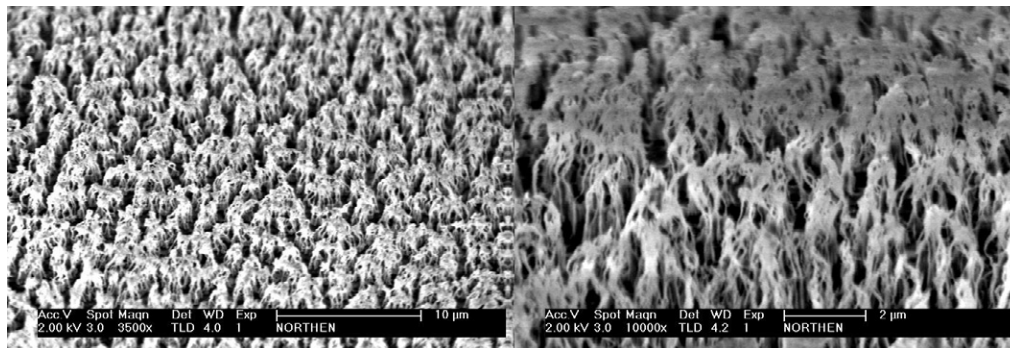


Figure 3. Organic looking polymeric nanorods, 'organorods', fabricated utilizing the instability of a dielectric in a large electric field. The ~ 100 nm features were achieved using a bilayer to reduce the interfacial energy, thus reducing the instability wavelength and corresponding feature size. Scale bars: 10 and 2 μm left and right respectively.

Following the platform and pillar fabrication, the photoresist surface (Shipley SPR 220-7, primarily composed of a diazoquinone ester and a phenolic novolak resin) of the platforms is transformed into organorods by placing it into an oxygen plasma with a 100 W bias for 5 min (figure 3), for a 3 cm \times 3 cm piece. Organorods have also been uniformly fabricated across a 100 mm silicon wafer. The bias creates an electric field gradient, which acting on the dielectric polymer induces a force large enough to overcome surface tension, causing the growth of vertical polymeric columns. Estimating the electric field across the photoresist to be $100 \text{ V } \mu\text{m}^{-1}$, a column size of around 1 μm is predicted [24], much larger than the 50–150 nm organorods. The reduced geometry of the organorods may be attributed to a bilayer of photoresist and hexamethyldisilazane (HMDS) decreasing the interfacial energy and shrinking the instability wavelength [25].

The use of a plasma induced electric field offers several advantages over a parallel plate induced field. Using a plasma to create the electric field requires no second electrode, and subsequently no precise control of the gap between the two plates. From a fabrication standpoint plasma induced nanorod growth utilizes already established processing infrastructure. Adopted from the IC community, and available on most

research campuses, plasma etching systems are convenient and established processing tools.

The most striking difference between the plasma growth of nanorods in this work and the parallel plate growth of nanorods performed by Schäffer *et al* is the reduced time it takes to form the nanostructures—5 min versus 18 h, respectively. In essence the plasma method offers a greatly accelerated growth mechanism; similar initial morphologies are seen before the formation of the organorods. A possible explanation for the greatly reduced formation time can be understood by examining the growth mechanism. Growth is caused by the electric field gradient exerting a force on the dielectric polymer. When this force exceeds the restoring force created by the surface tension of the polymer surface an undulated surface begins to appear and then transform into the polymeric pillars seen in figure 3 and reference [4]. In the plasma growth method the oxygen plasma serves to reduce the surface tension of the photoresist by breaking C–H bonds at the surface and leaving dangling –OH bonds. These dangling bonds reduce the surface tension, leaving the dielectric force to dominate over the restoring force, and organorods are formed.

To change the organorod surface from hydrophilic to hydrophobic the samples are placed in a CF_4 plasma for 30 s. This creates a fluorocarbon coating, increasing their

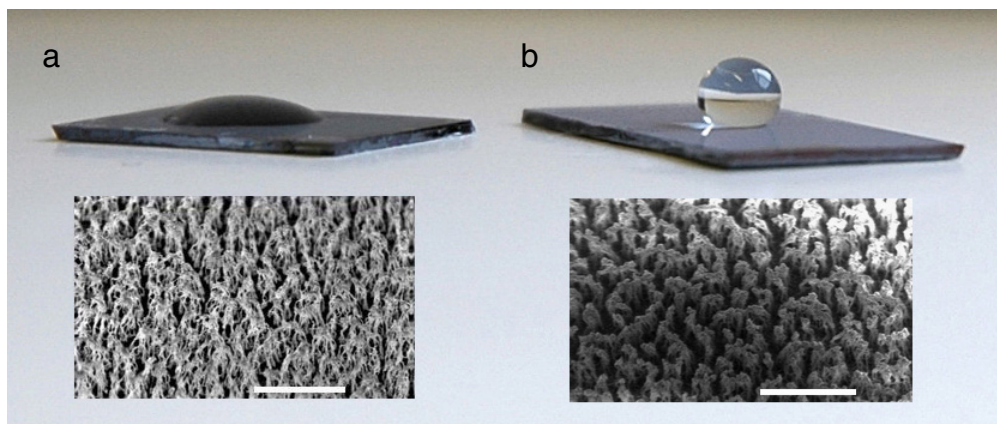


Figure 4. Comparison of hydrophilic and hydrophobic surfaces. (a) Top: water droplet partially wetting a hydrophilic organorod surface with a contact angle of $42.5^\circ \pm 2$ (top); bottom: electron micrograph of ~ 120 nm diameter organic looking nanorods, 'organorods'. Scale bar: $5 \mu\text{m}$. (b) Top: water droplet resting on top of the highly hydrophobic organorod surface with a contact angle of $145^\circ \pm 2$; bottom: electron micrograph shows the diameter of the organorods increased to ~ 350 nm from the fluorocarbon hydrophobic coating applied through plasma deposition. Scale bar: $5 \mu\text{m}$.

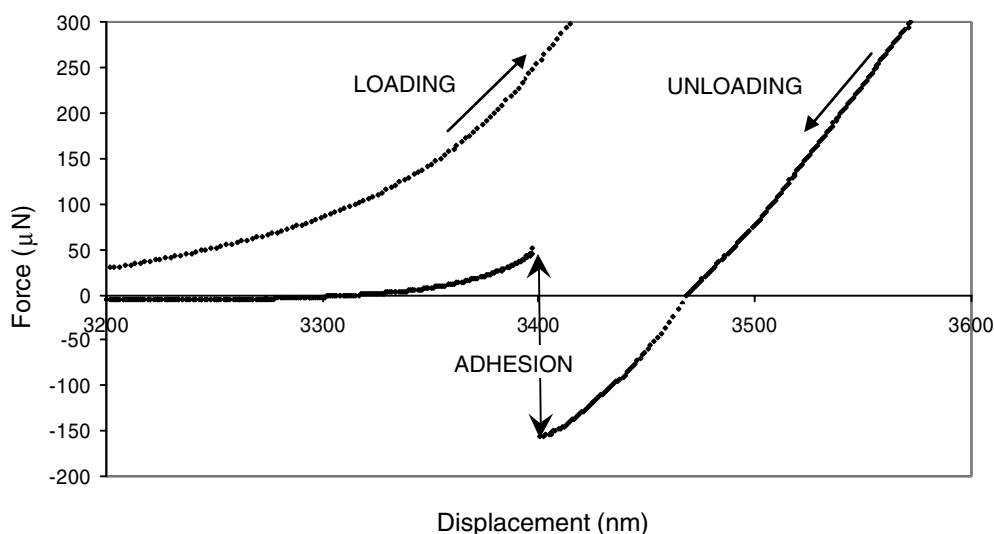


Figure 5. Typical nanoindenter adhesion test results for an organorod covered structure indented with a semi-rough 3.175 mm diameter spherical aluminium tip. The plot represents a typical load versus displacement curve illustrating loading, unloading, and pull-off adhesion.

size to ~ 350 nm, and altering their surface chemistry. The fluorocarbon coating leaves a $-\text{CF}_3$ terminated surface, greatly reducing the surface energy. Combining this coating with the morphology of the organorod surface creates a lotus leaf effect [26], making the surface highly hydrophobic with a water contact angle of $145^\circ \pm 2$ (figure 4).

3. Experimental details

Adhesion testing was performed using a Hysitron Triboindenter[®] with a 3.175 mm spherical aluminium tip (RMS roughness of $0.5 \mu\text{m}$ over a $200 \mu\text{m}$ square). This non-ideal aluminium tip was chosen to better simulate an actual working environment for the adhesive, e.g. sensor deployment on an aircraft. To simulate a mesoscale adhesion incident, the 'rough' tip was pressed into the test surfaces and withdrawn orthogonally from the surface at a constant rate. Operating

in displacement control, load versus displacement data were collected from the nanoindenter and analysed to determine the adhesion. Adhering surfaces would produce a distinctive pull-off behaviour, where the unloading curve would make a sudden jump (figure 5). The adhesive force was taken to be the difference between the minimum value right before pull-off and the next stabilized point (the instrumentation requires a finite time to stabilize after the sudden pull-off event).

To the authors' knowledge, this is the first time a test measuring orthogonal adhesion on the tens of micrometre to millimetre scale has been performed. Refinement of the technique will, we hope, bring about a universal mesoscale adhesion test. The orthogonal test technique measures the pure adhesive component of force, offering the opportunity for better standardization of adhesion testing. In contrast, lateral force measurements include a frictional force difficult to decouple from the adhesive force. The common peel test,

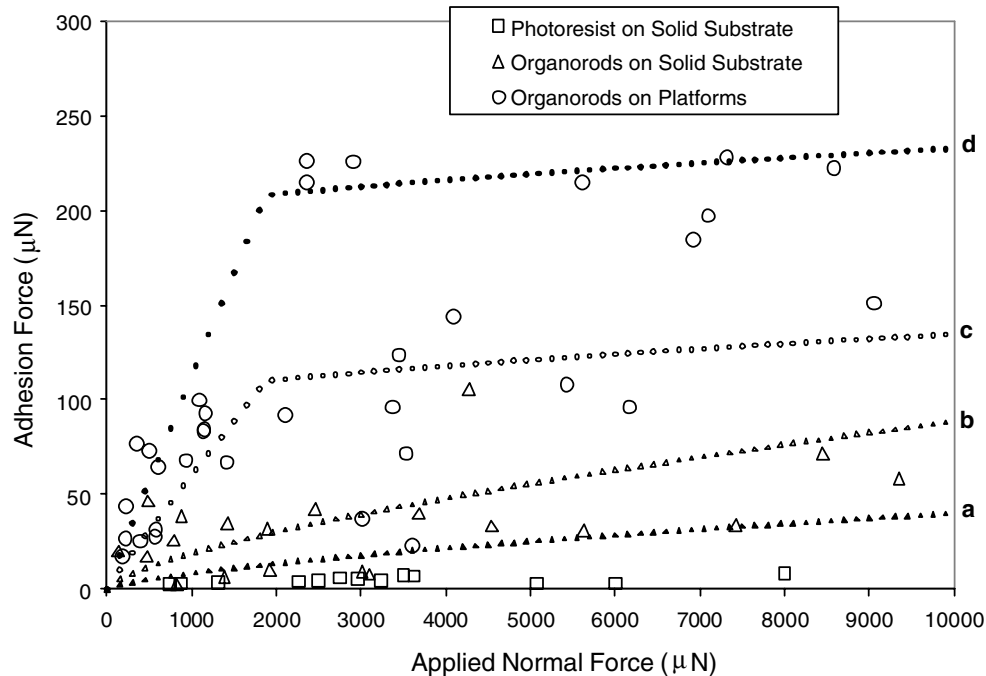


Figure 6. Nanoindenter adhesion testing results and theoretical models for hydrophilic polymeric surfaces. Test surfaces were indented with a semi-rough 3.175 mm diameter spherical aluminium tip. Increased normal loads created more surface contact between the spherical tip and surfaces, increasing adhesion. The organorod morphology enhanced surface adhesion over the solid photoresist surface. Adhesion was further enhanced by integration of organorods with flexible silicon dioxide platforms; large data scatter was a by-product of testing mesoscale adhesion with a rough surface. a, van der Waals and, b, Johnson–Kendal–Roberts (JKR) adhesion models predicting the collective adhesion of organorods over a given contact area, predicted by JKR contact mechanics for a sphere and flat surface. c, d, modified van der Waals adhesion accounting for increased contact area attributed to the conformation of platform ‘fingers’ with the test sphere: c, two fingers; d, four fingers. The saturation point corresponds to complete finger attachment; in the case of four fingers, d, this value nicely bounds the experimental data.

while useful for an industrial standard for tapes, also introduces variables again difficult to decouple from adhesion, e.g. rate and the effect of the support medium.

4. Results and discussion

The adhesive force was found to significantly depend on the maximum applied normal load (figures 6 and 7). This dependence is probably due to the increase in contact area between the two surfaces as a result of increased conformation, and deformation (plastic and elastic), of the adhesive to the spherical indenter surface. With hard flat substrates (e.g. silicon) clean loading and unloading curves were produced with no apparent adhesion. The photoresist surfaces demonstrated little adhesion (figure 6). In contrast, the organorod coated surfaces demonstrated much higher adhesion strengths (figure 6). Combining the organorods with the compliant pillar structures offered a significant increase in adhesion (figure 6), suggesting that the compliant structures aid in increasing the surface contact area. Initially it was anticipated that the pillar would allow the entire structure to rotate, aiding in surface conformation. However, with the millimetre scale of the aluminium sphere used in testing, only one structure is probably being tested and the compliance of the platform fingers are probably the dominant mechanism of conformal enhancement. As the aluminium sphere contacts the platform, the radial extending fingers are able to bend

up and contact the aluminium surface. This produces a near linear increase in adhesion with normal load. At some point, however, the finger (or fingers) is (are) completely in contact and can provide no further adhesion. Adhesion then becomes solely dependent on squashing the organorods in the centre of the structure (figure 8), and little increase in adhesion is seen thereafter.

To better mimic the structure and properties of the gecko tarsus a conformal hydrophobic fluorocarbon coating was deposited on the organorods. With the addition of the coating, contact angle measurements show a change from hydrophilic, $42.5^\circ \pm 2$, to highly hydrophobic, $145^\circ \pm 2$ (compared to $160.9^\circ \pm 1.4$ for the gecko [7]), behaviour with the fluorocarbon coating (figure 4). This change from hydrophilic to hydrophobic behaviour is not only significant in better mimicking the gecko adhesive structure, but may also shed new light on the purpose of the hydrophobic property. By testing the artificial adhesive before and after the addition of the hydrophobic coating, a comparison between hydrophilic and hydrophobic surface adhesion can be made, while with a gecko, it would be non-trivial to change the hydrophobic nature to perform a similar experiment. Surprisingly, adding a hydrophobic coating to the organorod surface improved the adhesion (figure 7). As will be discussed later, this result may be associated with factors other than just the change in surface composition, e.g. increased organorod size. Adhesion was further increased when the hydrophobic

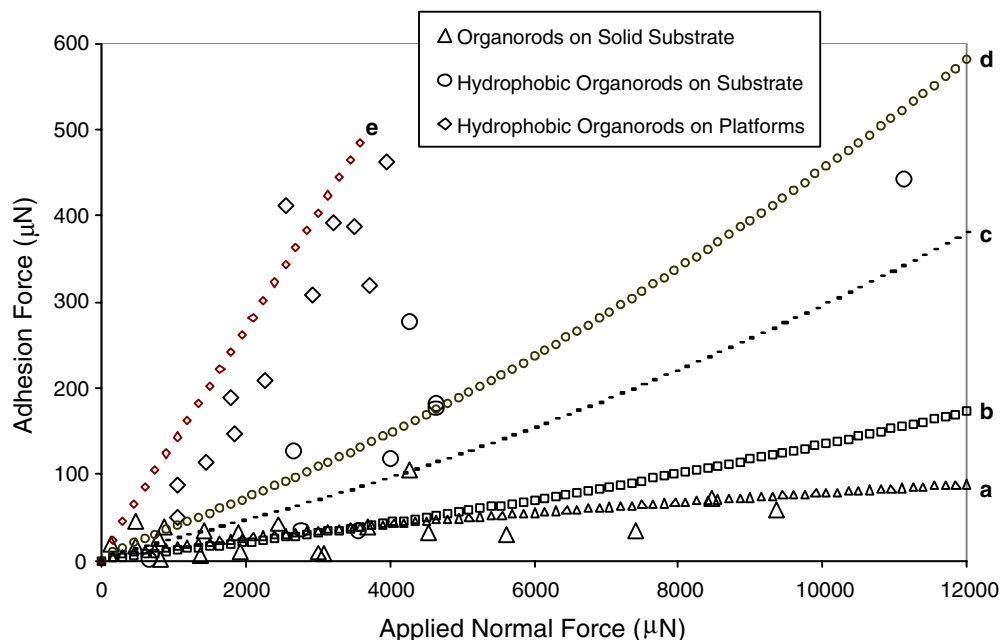


Figure 7. Nanoindenter adhesion testing results and theoretical models for hydrophobic polymeric surfaces. Surface adhesion between the sphere and test surfaces is enhanced by a hydrophobic coating on the organorods. The coating increases the size from ~ 120 to ~ 350 nm and reduces the surface energy. a, the van der Waals interaction energy model predicts an increase in adhesion with the larger organorods, but fails to capture the trend of the hydrophobic organorods. b, van der Waals and, c, JKR models compensating for an increased radius of curvature—determined by scanning electron microscopy—of organorods squashed during indentation show better agreement with experimental data. d, reduction of the interaction distance, d_0 , from 0.165 to 0.09 nm in the van der Waals model. e, combining the modified van der Waals models for hydrophobic organorods ($d_0 = 0.09$ nm) and the compliant platform model with one finger, excellent agreement with the mesoscale adhesion test is seen. Note the terminus of the dotted line represents one complete finger adhesion.

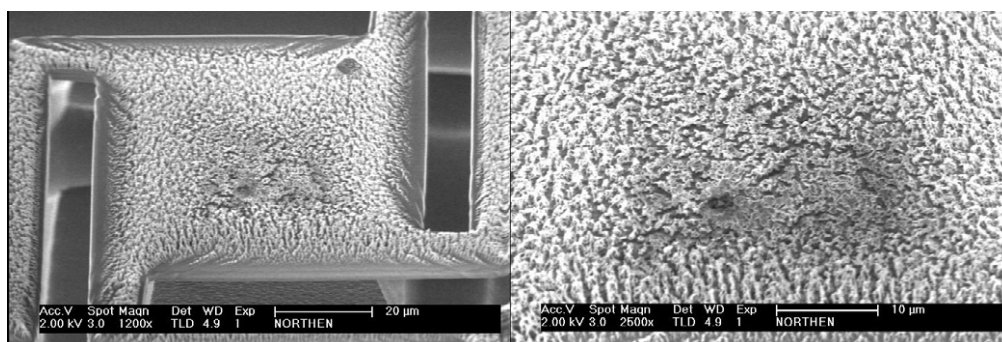


Figure 8. Scanning electron micrographs showing squashed organorods in the central portion of a structure. Scale bars: 20 and 10 μm left and right respectively.

organorods were combined with the compliant platform structures. Improved adhesion with the platforms may be a result of two mechanisms: one in which the fingers are improving the mesoscale surface conformation and the other occurring because the fingers are able to bend out of the plane changing the adhesion vector to include a transverse component.

Although the mechanism of the adhesion between the rough aluminium sphere and the organorod coated surfaces is quite complex—and many basic theoretical aspects of adhesion not fully understood—a simplified approach was taken to explain the experimental adhesion measurements. Two simple models based on Johnson–Kendall–Roberts (JKR) contact adhesion theory [27] and van der Waals interaction

forces [28] were used to capture the basic trend in adhesion seen. JKR theory for a sphere contacting a flat surface predicts a pull-off force of $F = (3/2)RW$, where R is the radius of the sphere and W is the work of adhesion, taken to be $\sqrt{\gamma_{\text{Al}}\gamma_{\text{polymer}}}$, where $\gamma_{\text{Al}} = 500 \text{ mJ m}^{-2}$ and $\gamma_{\text{polymer}} = 35 \text{ mJ m}^{-2}$ [29, 30]. For the organorod surface the radius of curvature of the rods is considered to be very small compared to the sphere (making the organorods the spherical contact surface and the aluminium sphere a flat surface) and the adhesion force is estimated to be $F_{\text{JKR}} = n(3/2)R_0W$, where R_0 is the diameter of the organorods (determined using scanning electron microscopy) and n is the number of organorods in contact with the surface—equal to the surface density of organorods multiplied by the contact area (determined using JKR contact mechanics for a

sphere contacting a flat surface [27] and verified using scanning electron microscopy).

Alternately, considering only the van der Waals contribution, the force is taken to be $F_{\text{vdW}} = HR_0/6d_0^2$, where H is the Hamaker constant (estimated to be $H = 2.1 \times 10^{-21} \text{ W} = 2.8 \times 10^{-19} \text{ J}$) [28], R_0 is the diameter of the organorods and d_0 is a characteristic cut-off distance equal to 0.165 nm [28]. As can be seen in figure 6, the JKR method tends toward the upper limit of values obtained in the rough aluminium sphere adhesion test (an overestimate of the actual number of organorods contributing to the adhesion), while the van der Waals method tends toward the lower limit (not accounting for other interaction forces, e.g. capillary forces).

Increased adhesion with the compliant platforms (figure 6) can be attributed to greater surface contact as a result of enhanced surface conformation, primarily due to the flexible platform fingers. The additional contact area of the fingers was assumed to increase linearly with the applied load and was included in the van der Waals model from above. The new model, for the case of two and four fingers adhering, was compared with the experimental data for the organorod covered flexible platforms (figure 6). Although there is a considerable amount of scatter, due in part to the nature of this 'real life' rough sphere test, there is good agreement between the predicted adhesion for all four fingers in contact and the maximum measured adhesion strengths. This also helps to understand the origin of much of the scatter. On every successive indent it is possible that not all the platform fingers are making contact—especially considering the roughness of the indenter tip. While this introduces a variance in the data and makes modelling tricky, from an application standpoint larger arrays will produce a conglomerate adhesive strength.

Addition of the hydrophobic coating to the organorod surface increased adhesion. It was expected that the decrease in surface energy with the hydrophobic coating would reduce the adhesion. The hydrophobic coating on the organorods increased the diameter of the organorods and changed the surface composition. Considering these two factors the van der Waals model was modified, with $R_0 = 350 \text{ nm}$ and $\gamma_{\text{polymer}} = 19 \text{ mJ m}^{-2}$ [29, 30], and plotted against the experimental data (figure 7). While the model predicts a slight increase in adhesion over the smaller organorods, it greatly underestimates the adhesion of the hydrophobic organorods. Further investigation using scanning electron microscopy revealed that the hydrophobic organorods tended to change conformation under applied pressure, effectively changing their radius of curvature. Both JKR and van der Waals models were modified to account for the increased size of the organorods (figure 7, lines b and c).

While the JKR model offered a better prediction, both models failed to capture the experimental data trend. Upon examination the van der Waals equation has a strong dependence on d_0 , the estimated cut-off distance—basically determining the range of interaction of van der Waals forces. Reducing the cut-off distance, d_0 , from 0.165 to 0.09 nm, the van der Waals model better represents the experimental data (figure 7, line d). This suggests that the hydrophobic coating may enhance the van der Waals adhesive force by decreasing the surface to surface interaction distance.

A composite model for the hydrophobic organorods on the flexible platforms was constructed by accounting for the

compliant fingers in the van der Waals hydrophobic organorod model, with $d_0 = 0.09 \text{ nm}$. Comparing this model with the experimental data, excellent agreement is seen (figure 7, line e). The slight lag in the experimental curve can be attributed to the delay in finger attachment (the sphere must press into the centre of the platform before it becomes sufficiently close to interact with the extended fingers). Note that the highest adhesion attainable experimentally, 462 μN , corresponds to one complete finger attachment (the end of line e in figure 7) and a predicted adhesion of 485 μN .

Some simple models for explaining a complex adhesion phenomenon have been presented. Although simple, the models do show reasonable agreement with the empirical data, although the testing was initially designed to produce only relative strengths of adhesion between the biomimetic adhesives and a rough aluminium sphere. The rough sphere testing introduces a significant amount of scatter into the data making analytical comparisons tenuous. However, the *relative* improvement in adhesion with the hydrophobic surface over the hydrophilic surface case is an intriguing result. To ascertain the mechanism of this adhesion improvement, and to support the validity of the testing, the nanoindenter testing should be repeated with a smooth and more ideal indenter surface—e.g. a polished flat punch tip. This would certainly help to eliminate much of the scatter and remove the adhesion strength dependence on the applied load, as is seen with the spherical tip.

5. Summary

Arrays of flexible silicon dioxide platforms supported by single high aspect ratio silicon pillars have been fabricated. These platforms, when coated with polymeric organorods, show a significant increase in adhesion over solid organorod covered substrates. Further improvement in adhesion is measured with the addition of a highly hydrophobic organorod surface—possibly enhancing van der Waals interactions. This indicates that the superhydrophobic nature of the gecko pad may serve to improve adhesion, instead of just aiding in self-cleaning and wear characteristics. Future work on the synthetic adhesive will focus on optimization of the structure, more ideal testing for theoretical purposes, and scaling up fabrication for macroscale testing and device integration.

Acknowledgments

We thank Marco Aimi, Masa Rao and Brian Thibeault for their valuable processing conversations; Laurent Pelletier, Michael Requa and Alicia Soliz for their constructive comments on previous drafts of this document. Funding was provided by AFOSR Contract Number FA9550-05-1-0045 and UCSB. Fabrication was carried out at Nanotech Nanofabrication Facility at UC Santa Barbara, part of the National Nanotechnology Infrastructure Network.

References

- [1] Madersson P F A 1964 Keratinized epidermal derivatives as an aid to climbing in gekkonid lizards *Nature* **203** 780–1

- [2] Hildebrand M 1988 *Analysis of Vertebrate Structure* 3rd edn (New York: Wiley) p 701
- [3] Hiller U 1975 Comparative studies on the functional morphology of two gekkonid lizards *J. Bombay Natural History Soc.* **73** 278–82
- [4] Ruibal R and Ernst V 1979 The structure of the digital setae of lizards *J. Morphol.* **117** 271–94
- [5] Williams E E and Peterson J A 1982 Convergent and alternative designs in the digital adhesive pads of scincid lizards *Science* **215** 1509–11
- [6] Autumn K *et al* 2000 Adhesive force of a single gecko foot-hair *Nature* **405** 681–5
- [7] Autumn K *et al* 2002 Evidence for van der Waals adhesion in gecko setae *Proc. Natl Acad. Sci.* **99** 12252–6
- [8] Gao H and Yao H 2004 Shape insensitive optimal adhesion of nanoscale fibrillar structures *Proc. Natl Acad. Sci.* **101** 7851–6
- [9] Scherge M and Gorb S 2001 *Biological Micro- and Nanotribology: Nature's Solutions* (Berlin: Springer)
- [10] Persson B N J and Gorb S 2003 The effect of surface roughness on the adhesion of elastic plates with application to biological systems *J. Chem. Phys.* **119** 11437–44
- [11] Persson B N J 2003 On the mechanism of adhesion in biological systems *J. Chem. Phys.* **118** 7614–21
- [12] Arzt E, Gorb S and Spolenak R 2003 From micro to nano contacts in biological attachment devices *Proc. Natl Acad. Sci.* **100** 10603–6
- [13] Sitti M and Fearing R 2003 Synthetic gecko foot-hair micro/nano-structures as dry adhesives *J. Adhesion Sci. Technol.* **18** 1055–74
- [14] Geim A K *et al* 2003 Microfabricated adhesive mimicking gecko foot-hair *Nat. Mater.* **2** 461–3
- [15] Senturia S D 2001 *Microsystem Design* (Dordrecht: Kluwer–Academic)
- [16] Boltshauser T and Baltes H 1991 Capacitive humidity sensors in SACMOS technology with moisture absorbing photosensitive polyimide *Euroensors IV '90 (Karlsruhe, West Germany)*
- [17] Davis Z J *et al* 2000 Fabrication and characterization of nanoresonating devices for mass detection *J. Vac. Sci. Technol. B* **18** 612–6
- [18] Ilic B *et al* 2000 Mechanical resonant immunospecific biological detector *Appl. Phys. Lett.* **77** 450–2
- [19] Kenny T 2001 Nanometer-scale force sensing with MEMS devices *IEEE Sensors J.* **1** 148–57
- [20] Lang H P, Berger H *et al* 1998 Sequential position readout from arrays of micromechanical cantilever sensors *Appl. Phys. Lett.* **72** 383–5
- [21] Thundat T *et al* 1995 Detection of mercury vapor using resonating microcantilevers *Appl. Phys. Lett.* **66** 1695–7
- [22] Zhang W, Baskaran R and Turner K L 2002 Effect of cubic nonlinearity on auto-parametrically amplified resonant MEMS mass sensor *Sensors Actuators A* **102/1-2** 139–50
- [23] Northen M T and Turner K L 2004 Single high aspect ratio pillar supports *ECS, The 206th Mtg of the Electrochemical Society* (Waikiki, HI: The Electrochemical Society)
- [24] Schäffer E, Thrun-Albrecht T, Russell T P and Steiner U 2000 Electrically induced structure formation and pattern transfer *Nature* **403** 874–7
- [25] Lin Z, Kerle T, Baker S M, Hoagland D A, Schäffer E, Steiner U and Russel T P 2001 Electric field induced instabilities at liquid/liquid interfaces *J. Chem. Phys.* **114** 2377–81
- [26] Nakajima A, Hashimoto K and Watanabe T 2001 Recent studies on super-hydrophobic films *Monatsh. Chem.* **132** 31
- [27] Johnson K L, Kendall K and Roberts A D 1971 Surface energy and the contact of elastic solids *Proc. R. Soc. A* **324** 310–3
- [28] Israelachvili J N 1992 *Intermolecular and Surface Forces* (New York: Academic)
- [29] El Ghzaoui A 1999 Determination of surface energy of polymers by force microscopy *J. Appl. Phys.* **85** 1231–3
- [30] Lieng-Huang L 1996 Correlation between Lewis acid–base surface interaction components and linear solvation energy relationship solvatochromic alpha and beta parameters *Langmuir* **12** 1681–7